Papers of Ship Research Institute VOL 27 NO.3 July 1990

Application of the Fractional Step Method to Free Surface Flow Problems *

By

Kyle D. Squires **, Takanori Hino *** and Yoshiaki Kodama ***

Abstract

In the first part of this paper, the fractional step method to solve the two-dimensional Navier-Stokes Equations for incompressible viscous fluid flow is presented. The developed code is validated by some simple flow programs such as the Tylor-Green problem of decaying vortices or the driven cavity flow problem. The extension of the method to free surface flow problems is then made. Issues such as grid generation, free surface boundary conditions and movement of the free surface in time are addressed. The troubles encountered in the application of the method to free surface flow problem are discussed and some recommendations for computaion of the free surface flow using the fractional step method are made.

Following these recommendations, the numerical method based on the MAC method is applied to free surface problems in the second part of the paper. The boundary and initial conditions for the generation of periodic progressive waves are discussed. The computational results show that the wave that has the given wave length and frequency can be generated by the proper boundary and initial conditions.

* Received on October 31, 1989
** Mechanical Engineering Department, Stanford University
*** Ship Performance Division

1. Introduction

Flows with free surfaces are important in many engineering applications. In particular, the surface flows around ships and other marine structures include many interesting fluid mechanical phenomena. One such phenomenon associated with these free surface flows is that of wave breaking. The breaking of waves about marine structures causes large impact loadings and leads to undesirable increases in drag on ships. Thus, a better understanding of the mechanisms involved with breaking waves will perhaps lead to improved design and construction of ships and other marine structures.

For engineering applications numerical solution of the governing equations is a useful tool for aiding in the design and construction of ships and marine structures. However, for engineering design and analysis the governing equations are averaged over time or space and thus the effects of turbulence must be incorporated into these averaged equations. This is the principal difficulty in using numerical approaches in that accurate turbulence models are required in order to obtain reliable predictions of the forces and flows about ships or other marine structures. Thus, it is very important that accurate and reliable turbulence models be used in these calculations.

In order to construct reliable turbulence models for free surface flows it is necessary to increase our basic understanding of these flows. The information required for these turbulence models has been traditionally obtained from laboratory experiments. However, with the advent of powerful and fast supercomputers the use of direct numerical simulation (DNS), or full simulation, has opened up a new approach for increasing basic understanding of many turbulence phenomena.

A full simulation is a calculation which produces an exact solution of the time-dependent, Navier-Stokes equations over the full range of relevant length scales down to the smallest scales of the turbulence. Such a simulation requires tremendous computer resources, but requires no time averaging of the governing equations nor any turbulence modelling. Therefore, the calculations can be treated as an experiment with accurate, time-dependent data available at a large number of locations.

Results obtained from full simulation can be used to support phenomenological turbulence modelling. The use of full simulation has provided new insight into the problem of turbulent dispersion (Lee, Squires, et.al. [1]). DNS has also been instrumental in learning about the structure of turbulent channel flow (Moser and Moin [2]). Certain statistical correlations needed for turbulence models are impossible to measure in laboratory experiments but very straightforward to obtain from the simulation data.

To date full simulation has been applied to canonical turbulent flows. Examples including isotropic turbulence, homogeneous turbulence, fully-developed flow in a channel, and flat-plate boundary layers. The geometry for each of these flows is simple and therefore very accurate numerical techniques may be applied to the computation of such a flow. Typically, spectral methods are used for the calculation of these flows. Spectral methods are much more accurate than traditional finite

difference techniques in that the high wave number components of the solution are much more accurately represented and there is no phase error for a spectral method.

Thus, to perform full simulations of free surface flows accurate numerical techniques must be devised and tested so that the results obtained from the simulations may be trusted. It is important that the numerical technique be as accurate as possible so that the solutions obtained from the simulations be relatively free from errors associated with the numerical approximation of the governing equations.

Since the governing equations for free surface flows are the incompressible Navier-Stokes equations the principal difficulty with obtaining time-accurate solutions arises from the fact that the continuity equation does not contain a time-derivative explicitly. Thus, the constraint of mass conservation is obtained through the coupling of the continuity equation and the pressure in the momentum equations. As pointed out by Kim and Moin [3], the fact that the continuity equation does not have a time derivative prevents the use of conventional alternating-direction-implicit (ADI) schemes for advancing the governing equations in time. Thus, one approach is to use the continuity equation along with the momentum equations to derive the Poisson equation for the pressure field. In this way, the elliptic nature of the calculation is expressed by a single equation. It is also important to note that the numerical scheme preserves such global quantities as mass, momentum, kinetic energy, and circulation since failure to do so can result in numerical instability.

The objective of this paper is to demonstrate the application of one method for solving the incompressible Navier-Stokes equations which satisfies global conservation of the above quantities. In the first part of this paper the fractional step method of Kim and Moin is described and results from the method are obtained for the Taylor-Green problem of decaying vortices and also flow in a driven cavity at four Reynolds numbers. Extension of the method to the free surface problem is then discussed. Issues such as grid generation, free surface boundary conditions, and movement of the free surface in time are addressed. The present work will provide more detail of the fractional step method of Kim and Moin and it is thus hoped the additional detail will be useful to future users of the method.

In the second part, the numerical method based on the MAC method is applied to free surface problems. The boundary and initial conditions for the generation of periodic progressive waves are discussed. The computational results show that the wave that has the pre-determined wave length and frequency can be generated by the proper boundary and initial conditions.

Part I. Fractional Step Method

2. Numerical Method

The method used for the results obtained in this paper is based on the fractional step method of Chorin [4] for time-advancement of the Navier-Stokes and continuity

equations for incompressible viscous flow:

$$\frac{\partial u_i}{\partial t} + \frac{\partial (u_i u_j)}{\partial x_j} = -\frac{\partial P}{\partial x_i} + \frac{1}{Re}\frac{\partial^2 u_i}{\partial x_j \partial x_j} \tag{2.1}$$

$$\frac{\partial u_i}{\partial x_i} = 0 \tag{2.2}$$

where both the dependent and independent variables have been appropriately non-dimensionalized.

Application of the fractional-step, or time-split, method to the incompressible Navier-Stokes equations is a "natural" choice for advancing the equations since the pressure field may be interpreted as a projection operator which projects an arbitrary velocity field onto a divergence free vector field. Thus, a two-step time-advancement scheme of equations (2.1) and (2.2) is

$$\frac{\hat{u}_i - u^n{}_i}{\delta t} = -\frac{\delta P^n}{\delta x_i} - \frac{3}{2}\frac{\delta (u_i u_j)^n}{\delta x_j}$$

$$+\frac{1}{2}\frac{\delta (u_i u_j)^{n-1}}{\delta x_j} + \frac{1}{2Re}\frac{\delta^2}{\delta x_j \delta x_j}(\hat{u}_i + u^n{}_i) \tag{2.3}$$

$$\frac{u^{n+1}{}_i - \hat{u}_i}{\delta t} = -\frac{\delta P^{n+1}}{\delta x_i}$$

$$+\frac{1}{2Re}\frac{\delta^2}{\delta x_j \delta x_j}(u^{n+1}{}_i - \hat{u}_i) + \frac{\delta P^n}{\delta x_i} \tag{2.4}$$

and

$$\frac{\delta u^{n+1}{}_i}{\delta x_i} = 0. \tag{2.5}$$

Note that by adding equations (2.3) and (2.4) the intermediate velocity field, $\hat{u}_i$, and the value of the pressure gradient at time level n vanish from the discrete approximation. The reason for subtracting the time level n pressure gradient from equation (2.3) and then adding it to equation (2.4) will become evident when boundary conditions for the intermediate velocity field are derived. The first fractional step (equation (2.3)) is a second order accurate approximation of the non-linear and viscous terms (second order explicit Adams-Bashforth for the non-linear terms and second order implicit Crank-Nicholson for the viscous terms). The second fractional step can be shown to be the correction, or projection, of the intermediate velocity field, $\hat{u}_i$, onto a divergence-free vector field by equating the divergence of a new variable, ϕ, with the right-hand side of equation (2.4):

$$-\frac{\delta \phi^{n+1}}{\delta x_i} = -\frac{\delta P^{n+1}}{\delta x_i} + \frac{1}{2Re}\frac{\delta^2}{\delta x_j \delta x_j}(u^{n+1}{}_i - \hat{u}_i) + \frac{\delta P^n}{\delta x_i} \tag{2.6}$$

thus the second fractional step may be rewritten as

$$\frac{u^{n+1}{}_i - \hat{u}_i}{\delta t} = -\frac{\delta \phi^{n+1}}{\delta x_i} \tag{2.7}$$

The pressure can be expressed in terms of this new variable ϕ through the following relations:

$$-\frac{\delta \phi^{n+1}}{\delta x_i} = -\frac{\delta \tilde{P}}{\delta x_i} + \frac{1}{2Re}\frac{\delta^2}{\delta x_j \delta x_j}(u^{n+1}{}_i - \hat{u}_i) \tag{2.8}$$

where

$$\tilde{P} = P^{n+1} - P^n. \tag{2.9}$$

Equation (2.7) can be used to express the second term on the right hand side of equation (2.8) in terms of ϕ and thus by integrating (2.8) one can show

$$\tilde{P} = \phi^{n+1} - \frac{\delta t}{2Re}\frac{\delta^2 \phi^{n+1}}{\delta x_j \delta x_j} \tag{2.10}$$

All spatial derivatives in (2.3) and (2.4) are expressed using second order accurate central differences on a fully staggered grid (Figure 1). For the staggered grid the continuity equation is enforced about the pressure nodes (in each cell) and the momentum equations are satisfied about the velocity nodes. Since a staggered grid is used, pressure boundary conditions are not required. It may also be shown that in the absence of time-differencing errors and viscosity, global conservation of momentum, kinetic energy, and circulation are preserved (Lilly [7]). The principal difficulty of using staggered grids is that some velocity components are not defined on the boundaries. Extension to higher orders of accuracy is also difficult.

To avoid the stability restriction imposed by the viscous terms an implicit time-advance scheme is used in equation (2.3). Rewriting the first fractional step

$$(1 - A_1 - A_2 - A_3)(\hat{u}_i - u^n{}_i) = \delta t\Big(-\frac{3}{2}\frac{\delta (u_i u_j)^n}{\delta x_j}$$

$$+\frac{1}{2}\frac{\delta (u_i u_j)^{n-1}}{\delta x_j} - \frac{\delta P^n}{\delta x_i}\Big) + 2(A_1 + A_2 + A_3)u^n{}_i \tag{2.11}$$

where $A_1 = (\delta t/2Re)(\delta^2/\delta x^2)$, $A_2 = (\delta t/2Re)(\delta^2/\delta y^2)$, $A_3 = (\delta t/2Re)(\delta^2/\delta z^2)$. To solve equation (2.11) requires the inversion of a large sparse matrix. For computations using a large number of grid points this is not practical so equation (2.11) is factored into the following form:

$$(1 - A_1)(1 - A_2)(1 - A_3)(\hat{u}_i - u^n{}_i) = \delta t\Big(-\frac{3}{2}\frac{\delta (u_i u_j)^n}{\delta x_j}$$

$$+\frac{1}{2}\frac{\delta (u_i u_j)^{n+1}}{\delta x_j} - \frac{\delta P^n}{\delta x_i}\Big) + 2(A_1 + A_2 + A_3)u^n{}_i. \tag{2.12}$$

In equation (2.12) terms of order δt^3 have been neglected but only inversion of tridiagonal matrices is required. One issue that arises in solving a factored system such as equation (2.12) is the boundary conditions for the intermediate velocity fields. To illustrate this consider the solution of the two dimensional problem:

$$(1 - A_1)(1 - A_2)(\hat{u}_{i,j} - {u^n}_{i,j}) =$$

$$\delta t f_{i,j} + 2(A_1 + A_2){u^n}_{i,j} \tag{2.13}$$

where $f_{i,j}$ are the non-linear terms advanced by second order Adams Bashforth and the pressure gradient evaluated at time level n in equation (2.12). For simplicity, rewrite the above equation as

$$(1 - A_1)(1 - A_2)\Delta u_{i,j} = RHS_{i,j}. \tag{2.14}$$

To solve the above rewrite the system as

$$(1 - A_2)\Delta u_{i,j} = \Delta {u'}_{i,j} \tag{2.15a}$$

$$(1 - A_1)\Delta {u'}_{i,j} = RHS_{i,j} \tag{2.15b}$$

Expanding the second step (equation (2.15b)):

$$\Big(1 - \frac{\delta t}{2Re}\frac{\delta^2}{\delta x^2}\Big)\Delta {u'}_{i,j} = RHS_{i,j} \tag{2.16}$$

$$\Delta {u'}_{i,j} - \frac{\delta t}{2Re\delta x^2}$$

$$\Big(\Delta {u'}_{i+1,j} - 2\Delta {u'}_{i,j} + \Delta {u'}_{i-1,j}\Big) = RHS_{i,j} \tag{2.17}$$

for an equally spaced grid in the x-direction. Defining $\beta = -\delta t/2Re\delta x^2$ equation (2.17) becomes

$$\beta\Delta {u'}_{i+1,j} + (1 - 2\beta)\Delta {u'}_{i,j} + \beta\Delta {u'}_{i-1,j} = RHS_{i,j}$$

$$i = 1, \ldots, NX$$

$$j = 1, \ldots, NY \tag{2.18}$$

Thus, boundary values are required for $\Delta {u'}_{0,j}$ and $\Delta {u'}_{NX+1,j}$. These boundary conditions are obtained from the second sweep, i.e., equation (2.15a). For example, at $i = 1$

$$\Delta {u'}_{0,j} = (1 - A_2)\Delta u_{0,j} \tag{2.19}$$

and expanding this gives

$$\Delta {u'}_{0,j} = \Delta u_{0,j} - \frac{\delta t}{2Re\delta y^2}(\Delta u_{0,j+1} - 2\Delta u_{0,j} + \Delta u_{0,j-1}). \tag{2.20}$$

It should be noted that by neglecting the second term on the right hand side of equation (2.20) the boundary conditions for the first sweep will be accurate to order δt^2.

The continuity equation, (equation (2.5)), and the second fractional step (equation (2.4)) may be used to obtain an equation for ϕ^{n+1}. Enforcing the continuity equation at time level $n+1$ and using equation (2.7) to express the new time level velocity in terms of ϕ^{n+1} yields the following:

$$\frac{\delta^2 \phi^{n+1}{}_{i,j}}{\delta x^2} + \frac{\delta^2 \phi^{n+1}{}_{i,j}}{\delta y^2} = \frac{1}{\delta t}\left(\frac{\delta \hat{u}_{i,j}}{\delta x} + \frac{\delta \hat{v}_{i,j}}{\delta y}\right) \tag{2.21}$$

for points away from the boundaries. For points near the boundaries the above equation is slightly modified by the velocity boundary conditions. For example, near the lower boundary the term $\delta^2\phi/\delta y^2$ is expressed as

$$\frac{\delta^2 \phi_{i,1}}{\delta y^2} = \frac{1}{\delta y}\left(\frac{\phi_{i,2} - \phi_{i,1}}{\delta y} - \frac{\phi_{i,1} - \phi_{i,0}}{\delta y}\right) \tag{2.22}$$

and using equation (2.7) this is

$$-\frac{\phi_{i,1} - \phi_{i,0}}{\delta y} = \frac{v^{n+1}{}_{i,1/2} - \hat{v}_{i,1/2}}{\delta t} \tag{2.23}$$

therefore

$$\frac{\delta^2 \phi_{i,1}}{\delta y^2} = \frac{1}{\delta y}\left(\frac{\phi_{i,2} - \phi_{i,1}}{\delta y} + \frac{v^{n+1}{}_{i,1/2} - \hat{v}_{i,1/2}}{\delta t}\right) \tag{2.24}$$

A solution to equation (2.21) may be obtained using transform methods. For the two-dimensional problem with a uniform grid spacing in the x direction the value of $\phi^{n+1}{}_{i,j}$ may be expressed as

$$\phi^{n+1}{}_{i,j} = \sum_{l=1}^{NX} \hat{\phi}_{l,j} \cos\left(\frac{\pi l}{NX}(i - \frac{1}{2})\right) \tag{2.25}$$

Using this in equation (2.21) and the orthogonality property of cosines one can obtain

$$\frac{\delta^2 \hat{\phi}_{l,j}}{\delta y^2} - k'_l \hat{\phi}_{l,j} = \hat{Q}_{l,j} \tag{2.26}$$

where $k'_l = 2(1 - \cos(\pi l/\mathrm{NX}))/\delta \mathrm{x}^2$ is the modified wave number for central differences and $\hat{Q}_{l,j}$ is the transformed source term. Thus, for each wave number a tridiagonal matrix is inverted to obtain the values of the coefficients of that wave number. The zeroth wave number is a special case and must be handled differently since the tridiagonal matrix for $k'_l = 0$ is singular. For this case equation (2.26) is

$$\frac{\delta^2 \hat{\phi}_{l,j}}{\delta y^2} = \hat{Q}_{l,j} \tag{2.27}$$

and for an equally spaced grid in the y-direction this equation applied at node j yields the value of $\hat{\phi}_{0,j+1}$

$$\hat{\phi}_{0,j+1} = \delta y^2 \hat{Q}_{0,j} + 2\hat{\phi}_{0,j} - \hat{\phi}_{0,j-1} \tag{2.28}$$

for $j = 1, \ldots, NY - 1$. The value of $\hat{\phi}_{0,1}$ is obtained from the boundary data. From equation (2.7)

$$\frac{\delta \hat{\phi}_{0,1}}{\delta y} = \hat{a} \tag{2.29}$$

where

$$-\hat{a} = \frac{\hat{v}^{n+1}_{0,1/2} - \hat{v}_{0,1/2}}{\delta t} \tag{2.30}$$

thus

$$\hat{\phi}_{0,1} = \hat{\phi}_{0,0} + \delta y \hat{a}. \tag{2.31}$$

Arbitrarily choosing $\hat{\phi}_{0,0}$ to be zero allows determination of $\phi_{0,1}$ from (2.31) and the rest of the zeroth mode coefficients from equation (2.27). It should be remarked that this method of solution is entirely consistent with the solution of the Poisson equation with Neumann boundary conditions. For additional details see Kim and Moin [3] and Peyret and Taylor [5].

The cosine series shown in equation (2.25) accounts for the fact that grid is staggered, i.e., pressure is not defined on the boundaries of the domain. Thus, the actual implementation of equation (2.25) is complicated by this fact and further manipulations must be done in order to use fast transforms to compute the coefficients of the series. Appendix A describes the steps necessary to use fast transform methods to compute the coefficients in equation (2.25). It should also be remarked that the use of trigonometric expansion such as that shown in equation (2.25) is valid only for an equally spaced grid in the x-direction. Thus, for complex geometries one would have to resort to iterative methods such as SOR or multi-grid for obtaining a solution of the Poisson equation.

Finally, given the new values of ϕ^{n+1} obtained using the relations shown above the new time level velocities may be calculated from equation (2.7).

2.1 Boundary Conditions for Intermediate Velocity Field

For fractional step methods boundary conditions for the intermediate velocity field are required for the tridiagonal matrix inversion in equation (2.12). It should be noted that for an explicit time advancement of the governing equations the solution at the new time level is *independent* of the boundary values of the intermediate velocity field (see Peyret and Taylor [5] for further discussion). The boundary conditions used for the intermediate velocity fields for the results shown in this paper are slightly different than those of Kim and Moin [3].

As shown by Kim and Moin, to construct proper boundary conditions for $\hat{u}_i$, it is regarded as an approximation to u^*_i where the continuous function satisfies

$$\frac{\partial u^*_i}{\partial t} = -\frac{\partial u^*_i u^*_j}{\partial x_j} + \frac{1}{Re}\frac{\partial^2 u^*_i}{\partial x_j \partial x_j} - \frac{\partial P^*}{\partial x_i} \tag{2.1.1}$$

following Kim and Moin,

$$\begin{aligned}\hat{u}_i \approx u^*_i(\mathbf{x}, t_n + \delta t) &= u^*_i(\mathbf{x}, t_n) + \delta t \frac{\partial u^*_i}{\partial t} + \frac{1}{2}\delta t^2 \frac{\partial^2 u^*_i}{\partial t^2} \\ &= u^*_i(\mathbf{x}, t_n) + \delta t\Big[-\frac{\partial u^*_i u^*_j}{\partial x_j} + \frac{1}{Re}\frac{\partial^2 u^*_i}{\partial x_j \partial x_j} - \frac{\partial P^*}{\partial x_i}\Big] \\ &+ \frac{1}{2}\delta t^2 \frac{\partial}{\partial t}\Big[-\frac{\partial u^*_i u^*_j}{\partial x_j} + \frac{1}{Re}\frac{\partial^2 u^*_i}{\partial x_j \partial x_j} - \frac{\partial P^*}{\partial x_i}\Big]\end{aligned} \tag{2.1.2}$$

Since $u^*_i(\mathbf{x}, t_n) = u_i(\mathbf{x}, t_n)$,

$$\begin{aligned}\hat{u}_i &= u_i(\mathbf{x}, t_n) + \delta t\Big[-\frac{\partial u_i u_j}{\partial x_j} + \frac{1}{Re}\frac{\partial^2 u_i}{\partial x_j \partial x_j} - \frac{\partial P}{\partial x_i}\Big] \\ &+ O(\delta t^2) = u_i(\mathbf{x}, t_n) + \delta t \frac{\partial u_i}{\partial t} + O(\delta t^2) \\ &= u_i(\mathbf{x}, t_{n+1}) + O(\delta t^2)\end{aligned} \tag{2.1.3}$$

thus, boundary conditions accurate to order δt^2 are obtained. The significant difference between the above derivation of the boundary conditions and that done by Kim and Moin is that the pressure gradient at time level n has been included in equation (2.3). Thus, the final result (equation (2.1.3)) is a more simple approximation of the boundary conditions than that obtained by Kim and Moin. Kim and Moin's result is

$$\hat{u}_i = u_i(\mathbf{x}, t_{n+1}) + \delta t \frac{\partial P}{\partial x_i} + O(\delta t^2) \tag{2.1.4}$$

For a staggered grid the pressure gradient is not available along the boundaries and must therefore be extrapolated from the interior points.

3. Numerical Checks of the Method

To test the various parts of the method such as the implicit treatment of the viscous terms, boundary conditions of the intermediate velocity field, etc. the Taylor-Green problem of decaying vortices was computed. This two-dimensional unsteady flow is a solution to the Navier-Stokes and continuity equation

$$u(x, y; t) = -\cos(x)\sin(y)e^{-2t} \tag{3.1a}$$

$$v(x, y; t) = -\sin(x)\cos(y)e^{-2t} \tag{3.1b}$$

$$P(x,y;t) = \frac{-1}{4}\big(\cos(2x) + \cos(2y)\big)e^{-4t} \tag{3.1c}$$

Errors in the u-component of velocity from two calculations using a different number of grid points are shown in Table 1. As expected, increasing the number of grid points decreases the error. These results also show the spatial differencing scheme is second order accurate.

The implicit part of the method was checked by integrating the following equations

$$\frac{\partial u}{\partial t} = -\frac{\partial P}{\partial x} + \frac{1}{Re}\nabla^2 u \tag{3.2a}$$

$$\frac{\partial v}{\partial t} = -\frac{\partial P}{\partial y} + \frac{1}{Re}\nabla^2 v \tag{3.2b}$$

$$\frac{\partial u}{\partial x} + \frac{\partial v}{\partial y} = 0. \tag{3.2c}$$

Since the non-linear terms have been eliminated, solution of the above equations should be independent of the time step if the time-advance scheme is unconditionally stable. It was found that stable solutions were obtained using time steps as large as $\delta t/(Re\delta x^2) = 10^4$ using the boundary conditions for the intermediate velocity field given by equation (2.1.3). It was also found that for computations of the cavity flow *with* the non-linear terms the steady state solutions obtained using an implicit treatment of the viscous terms were identical to solutions obtained using an explicit treatment of the viscous terms, giving another indication that the boundary conditions for the intermediate velocity field are consistent. It should be noted, however, that the boundary conditions given by equation (2.1.3) presume the values of the velocity field are known at the new time level. For flows that do not have a steady state solution (e.g., turbulence) this may not be true and this may affect the stability of the method. As mentioned previously, one disadvantage of the staggered grid approach is that some velocity components are not defined on the computational boundaries. Thus, to enforce boundary conditions such as no-slip a fictitious point outside of the boundary is used (see Figure 2). Since the value of this velocity is not known at time level $n+1$, it is approximated as the value from time level n. One alternative to such a procedure is to move the fictitious point to the boundary of the domain. The advantage of moving the points to the boundaries of the domain is that the boundary values are known, of course. However, for such a grid the order of accuracy of the spatial differencing scheme is first order along the boundaries (see Peyret and Taylor for further discussion). The code using the fractional step method outlined above was modified such that both the u and v velocity components were defined on the boundaries and for the driven cavity flow the results are virtually identical. It was found that steady state solutions were obtained in fewer iterations when the velocity points are defined on all boundaries. Thus, it is preferred to define velocity components on all boundaries at the sacrifice of accuracy near the boundaries.

As a final check of the method the flow in a driven cavity was computed. The flow in a driven cavity has long been a standard test problem for Navier-Stokes solvers. Since a large number of investigators have applied their codes to this problem there is general agreement of the results for Reynolds numbers up to 10000. It should also be mentioned that flow in a driven cavity becomes three-dimensional at moderately low Reynolds numbers (around Re=1000) and thus two-dimensional simulations of this flow at high Reynolds numbers are only of use as a test problem for Navier-Stokes solvers.

For this flow the upper wall of the cavity is moved at a constant velocity to the right ($u_{wall} = 1$) and the resulting flow field consists of several standing vortices, whose characteristics are functions of the Reynolds number. Figure 3 shows streamline contours for four different Reynolds numbers. It can be seen from the Figure that as the Reynolds number is increased the streamline pattern becomes more asymmetric. Vorticity contours are plotted in Figure 4 and again show this increasing asymmetry with increasing Reynolds number. At $Re = 1$ the flow field is virtually symmetric about the centerplane. Figure 5 shows the u-velocity profile along the cavity centerplane for $Re = 1$ from calculations using a 21 × 21 grid and a 31 × 31 grid. It can be seen the two velocity profiles are nearly converged. Another calculation was done using a 31 × 31($Re = 1$) grid but with a clustering of points near the upper and lower walls in order to check the results for a non-unform grid. The mapping of the uniform grid to the non-uniform grid in the y-direction for this calculation was

$$y_j = L_y \frac{(\beta+1)\left[\frac{(\beta+1)}{(\beta-1)}\right]^{(2y_j-1)} - \beta + 1}{2\left(1+\left[\frac{(\beta+1)}{(\beta-1)}\right]^{(2y_j-1)}\right)} \tag{3.3}$$

(see Anderson, Tannehill, and Pletcher [6] for further details).

The velocity profiles from a uniform grid calculation and the non-uniform grid calculation are shown in Figure 6. It can be seen there is a reasonable convergence in the results from the two calculations. Velocity profiles from the centerplane of the cavity for the four different Reynolds numbers used in the calculation are shown in Figure 7. This Figure shows the increase in the velocity gradient with increasing Reynolds number. Finally, in Table 2 are shown values of the stream function and vorticity at the center of the primary vortex for the different Reynolds numbers used in these calculations. Also shown in the table are values of these quantities obtained from the simulations done by other investigators. It can be seen from the table that the agreement between the results obtained from these simulations and those of other investigators is excellent.

4. Extension of the Fractional Step Method to the Free Surface Problem

The fractional step method described above was applied to the simulation of the two-dimensional free surface flow shown in Figure 8. Periodic boundary conditions were applied at the east/west boundaries and zero-gradient conditions were applied

along the lower boundary. Various boundary conditions were applied to the velocities in the cells containing the free surface such as extrapolation and the constraint of incompressibility. As was mentioned earlier, it is desirable that the numerical method be as accurate as possible. One reason for using periodic boundary conditions is that the solution may be expanded in a Fourier series (whose convergence properties are much better than finite differences). It was found, however, that for the free surface problem outlined in Figure 8 the use of a spectral method is very difficult and therefore a finite difference scheme was used.

To apply the fractional step method to the free surface problem as outlined with the given boundary conditions certain modifications must be made to the method. The most significant modification, of course, is the treatment of the free surface. Aside from the velocity and pressure fields an additional unknown is introduced into this problem: the height of the free surface. There are two approaches for time advancing the height of the free surface, a Lagrangian and an Eulerian method. In the Lagrangian approach marker particles on the free surface are tracked and in this way the location of the free surface is known at all times. This approach was originally used by Harlow and Welch [9] in applying their Marker-and-Cell technique to calculating free surface flows and has been successfully applied by other investigators as well. The principal drawback of this method for following the free surface is that it must be located within the computational domain at all times and thus there will always be some amount of wasted storage of the points above the surface which are devoid of fluid. In the Eulerian approach to determining the location of the free surface the differential equation for the surface height is solved along with the momentum and continuity equations and thus the free surface height is advanced in time in a similar fashion as the velocity field (for example Hino [10]). This approach has the advantage that there is no wasted storage when a body-fitted coordinate system is used in which the free surface is always located along the upper boundary of the computational domain. Since a body-fitted coordinate system is used the governing equations must now be mapped from the Cartesian grid (x, y) to the body-fitted coordinate system (ξ, η). The mapped equations written in conservation law form are

$$\frac{\partial}{\partial t}(\frac{q}{J}) + \hat{F}_\xi + \hat{G}_\eta = 0 \tag{4.1}$$

where

$$\begin{aligned} \hat{F} &= \frac{\xi_t}{J} q + \frac{\xi_x}{J} F + \frac{\xi_y}{J} G \\ \hat{G} &= \frac{\eta_t}{J} q + \frac{\eta_x}{J} F + \frac{\eta_y}{J} G \end{aligned} \tag{4.2}$$

(J is the Jacobian of the transformation). The height of the free surface, $h(x;t)$ is given by

$$\frac{\partial h}{\partial t} = -u\xi_x \frac{\partial h}{\partial \xi} + v \tag{4.3}$$

The vector of dependent variables, q, and flux vectors are given by:

$$q = \begin{bmatrix} u \\ v \\ 0 \end{bmatrix} \quad F = \begin{bmatrix} u^2 + p - \tau_{xx} \\ uv - \tau_{xy} \\ u \end{bmatrix}$$

$$G = \begin{bmatrix} uv - \tau_{xy} \\ v^2 + p - \tau_{yy} \\ v \end{bmatrix} \tag{4.4}$$

and the shear stresses are expressed as

$$\tau_{xx} = (\frac{1}{Re} + \nu_t)2u_x \ , \quad \tau_{xy} = (\frac{1}{Re} + \nu_t)\ (u_y + v_x)$$
$$\tau_{yy} = (\frac{1}{Re} + \nu_t)2v_y \qquad (4.5)$$

For the free surface problem the coordinate transformations are time-dependent since the grid follows the surface and thus the mapped flux vectors, $\hat{F}, \hat{G}$ are modifed accordingly. For the geometry shown in Figure 8 the following coordinate transformation was used:

$$\xi = \xi(x) = x \tag{4.6a}$$

$$\eta = \eta(x, y; t) = \frac{y}{h(x; t)} \tag{4.6b}$$

Equations (4.1) and (4.3) were solved using second order Runge-Kutta. Since the grid locations are time-dependent proper care must be exercised to ensure that the correct time levels of the metrics are used in updating the momentum equations, solving the Poisson equation for pressure, etc. This is more difficult when a staggered grid is used since separate metrics for the u and v momentum equations and the continuity equation must be stored.

Aside from solving the governing equations in the mapped ξ, η domain the treatment of the boundary conditions along the free surface must be addressed. For the free surface problem pressure boundary conditions are naturally specified along the surface. However, for the fractional step method on a staggered grid boundary conditions for the pressure field are not required. The pressure is a scalar quantity that is obtained to enforce the divergence-free constraint. Thus it is critical that the pressure calculated from the Poisson equation maintain the divergence-free condition of the velocity field since failure to do so may result in instability of the numerical method. This is especially important in a method that does not introduce artificial dissipation either through upwind differencing of the convective terms or the explicit use of extra dissipative terms in the governing equations. For the fractional step method described above there is no introduction of artificial dissipation. At first glance, it may also appear there is some inconsistency in specifying pressure boundary conditions along the free surface and then forcing the pressure field determined using these boundary conditions to enforce the continuity constraint. However, it

is important to keep in mind that the level of pressure is not important, only the difference (i.e., the gradient). However as will be shown, there is some ambiguity in the derivation of the Poisson equation which makes it difficult to enforce the divergence free constraint for the free surface problem when a time-dependent grid is used to follow the surface. For the free surface problem the pressure is re-defined to include the hydrostatic component, i.e.,

$$P^* = P + gy. \tag{4.7}$$

Thus, boundary conditions for the variable P^* are given by equation (4.7). For small surface curvature the static pressure, P, can be approximated by (Hirt and Shannon)

$$P = 2\nu \frac{\partial u_n}{\partial n} \tag{4.8}$$

where n is the local outward normal direction of the free surface.

Another important issue that arises in solving the governing equations on a non-uniform grid is the averaging that is required in computing the non-linear terms in the momentum equations. For a uniform grid the term $\delta uu/\delta x$ in the x-momentum equation is approximated on the staggered grid using second order accurate central differences as follows:

$$\frac{\delta(uu)_{i,j}}{\delta x} = \frac{1}{\delta x}\left[\frac{(u_{i+1,j} + u_{i,j})^2}{2} - \frac{(u_{i,j} + u_{i-1,j})^2}{2}\right]. \tag{4.9}$$

On a non-uniform grid there will be a loss of accuracy if the above formula is used to compute the averages for the non-linear terms. Thus it is necessary to use area-weighted averages for these terms. For highly skewed grids it may be necessary to include more of the neighboring points in computing the averages.

However, as mentioned above, a more critical aspect of solving the governing equations on a non-uniform grid is the derivation and solution of the Poisson equation and subsequent enforcement of the divergence-free constraint. For the coordinate mapping given by equations (4.6a) and (4.6b) the continuity equation is

$$\frac{\partial}{\partial \xi}\left(\frac{\xi_x}{J}u\right) + \frac{\partial}{\partial \eta}\left(\frac{\eta_x}{J}u\right) + \frac{\partial}{\partial \eta}\left(\frac{\eta_y}{J}v\right) = 0 \tag{4.10}$$

From section 2 it was shown that the second fractional step is used to derive the Poisson equation for pressure. For the mapping given by equations (4.6a, b) the second fractional step is given by:

$$\frac{u_{i,j}^{n+1}/J - \hat{u}_{i,j}/J}{\delta t} = -\frac{\delta}{\delta \xi}\left(\frac{\xi_x}{J}P_{i,j}\right) - \frac{\delta}{\delta \eta}\left(\frac{\eta_x}{J}P_{i,j}\right) \tag{4.11a}$$

$$\frac{v_{i,j}^{n+1}/J - \hat{v}_{i,j}/J}{\delta t} = -\frac{\delta}{\delta \eta}\left(\frac{\eta_y}{J}P_{i,j}\right) \tag{4.11b}$$

Notice that in equation (4.10) the quantity $\delta(\eta_x u/J)/\delta\eta$ is required. Since the continuity equation is enforced about the pressure nodes this quantity is not available at the grid points $i, j+1/2$ and $i, j-1/2$ and must be obtained from averages of the neighboring points. This averaging must be done such that the divergence-free constraint is satisfied. This also presents a difficulty in solving the Poisson equation The Poisson equation is

$$\frac{\delta}{\delta\xi}(\xi_x\frac{\delta}{\delta\xi}(\frac{\xi_x P}{J}))+\frac{\delta}{\delta\xi}(\xi_x\frac{\delta}{\delta\eta}(\frac{\eta_x P}{J}))+\frac{\delta}{\delta\eta}(\eta_x\frac{\delta}{\delta\xi}(\frac{\xi_x P}{J}))+$$
$$\frac{\delta}{\delta\eta}(\eta_x\frac{\delta}{\delta\eta}(\frac{\eta_x P}{J}))+\frac{\delta}{\delta\eta}(\eta_y\frac{\delta}{\delta\eta}(\frac{\eta_y P}{J}))=$$
$$\frac{\partial}{\partial\xi}\Big(\frac{\xi_x}{J}\hat{u}\Big)+\frac{\partial}{\partial\eta}\Big(\frac{\eta_x}{J}\hat{u}\Big)+\frac{\partial}{\partial\eta}\Big(\frac{\eta_y}{J}\hat{v}\Big) \tag{4.12}$$

The principal difficulty in solving the above equation is the appearance of the mixed derivatives. There are two possible alternatives to computing these terms. For example, consider the evaluation of the second term on the left hand side of equation (4.12) One possible evaluation of this term would be

$$\frac{\delta}{\delta\xi}(\xi_x\frac{\delta}{\delta\eta}(\frac{\eta_x P}{J}))=$$
$$\frac{1}{2\Delta\xi}\Big(\frac{\xi_{i+1,j}}{2\Delta\eta}(\frac{\eta_x}{J}P_{i+1,j+1}-\frac{\eta_x}{J}P_{i+1,j-1})$$
$$-\frac{\xi_{i-1,j}}{2\Delta\eta}(\frac{\eta_x}{J}P_{i-1,j+1}-\frac{\eta_x}{J}P_{i-1,j-1})\Big) \tag{4.13}$$

Notice that this approximation does not make any use of the information of the pressure at point i, j. Thus, another possibility for calculating the mixed derivative is to use average values, i.e.

$$\frac{\delta}{\delta\xi}(\xi_x\frac{\delta}{\delta\eta}(\frac{\eta_x P}{J}))=$$
$$\frac{1}{\Delta\xi}\Big(\frac{\xi_{i+1/2,j}}{\Delta\eta}(\frac{\eta_x}{J}P_{i+1/2,j+1/2}-\frac{\eta_x}{J}P_{i+1/2,j-1/2})$$
$$-\frac{\xi_{i-1/2,j}}{\Delta\eta}(\frac{\eta_x}{J}P_{i-1/2,j+1/2}-\frac{\eta_x}{J}P_{i-1/2,j-1/2})\Big) \tag{4.14}$$

where quantities such as $P_{i+1/2,j-1/2}$ are obtained from averages of the neighboring points. However, if averages are used to compute these values some type of area weighting should be used. The use of equation (4.14) also has the disadvantage in that the average values must be continuously updated in an iterative procedure. Since a non-uniform grid is used to for solving the free surface problem the use of trigonometric expansions can no longer be used for solving the Poisson equation and one has to resort to more traditional iterative methods for determining the pressure, such as Successive-Over-Relaxation.

Finally, since the grid is time-dependent the correct time levels of the metrics must be used. In the fractional step method the pressure is calculated at the new time level based on the velocities at the previous time level. It is not clear what effect the different time levels of the metrics will have on the subsequent enforcement of the divergence-free constraint.

It was found that the fractional step method applied to the free surface problem shown in Figure 8 did not yield stable solutions in time. It is believed the principal reason stable solutions could not be obtained is the difficulty in maintaining the conservation properties of the governing equations on the time-dependent non-uniform grid. It was also found through the course of the calculations that the divergence-free constraint was not satisfied, thus solution of the Poisson equation did not yield a pressure field that would in turn produced a divergence free velocity field. As previously mentioned this is probably due to the ambiguity in the derivation of the Poisson equation. The divergence of the velocity field was found to be the largest in the cells nearest the free surface. This is probably because of the choice of boundary conditions for the velocities in the cells containing the free surface. Boundary conditions such as zero-extrapolation do not give a velocity divergence of zero in the cells containing the free surface and this adversely effects the velocities in the adjacent cells.

4.1 Recommendations for computation of the free surface problem using the fractional step method

The use of the Lagrangian approach in obtaining the surface height has been successfully used by other investigators in simulating free surface problems. A distinct advantage of this approach is that the computational grid does not change in time. Thus problems with averaging to compute the non-linear terms do not arise and derivation of the Poisson equation is very straightforward (for a uniform grid calculation). This approach is perhaps more computationally efficient since the grid does not need to be re-generated at every time step. Therefore the first recommendation for future work is to use the fractional step method on a fixed grid with marker particles to track the height of the free surface. This approach would be very similar to Harlow and Welch's early calculations of free surface flows. An advantage of this approach is, that since a fixed grid system is used, spectral differencing may be possible in the periodic direction. This would be an excellent feature of a method that would be used for turbulence simulation since this would decrease the errors associated with the numerical approximation of the Navier-Stokes equations.

Part II. Free Surface Flow Simulation

In part I the fractional step method for the incompressible Navier-Stokes equations is applied to the free surface problem. However, for some reasons the steady solution cannnot be obtained. In this part, following the recomendations made in part I, another numerical method to solve free surface problems using a fixed grid is described. The numerical scheme used here is the MAC method which is based on the basically same concept as the fractional step method to satisfy the divergence-free condition with pressure correction. The numerical results for the generation of periodic progressive wave are also shown.

5. Numerical Method

5.1 Governing Equations and Basic Algorithm

The governing equations are the two dimensional Navier-Stokes equations (2.1) and the continuity equation (2.2) for the incompressible fluid.

The general curvilinear coordinates system (ξ, η) is introduced to use the non-uniform grid. This computational coordinates do not fit to the free surface shape. The free surface configuration is determined by the nonlinear kinematic free surface condition. The coordinates transformation is given as follows;

$$\xi = \xi(x, y), \eta = \eta(x, y), t = t \tag{5.1}$$

The momentum equations (2.1) and the continuity equation (2.2) are transformed through equation (5.1) as;

$$\begin{aligned} &u_t + Uu_\xi + Vu_\eta \\ &= -(\xi_x p^*_\xi + \eta_x p^*_\eta) + \frac{1}{Re}(\nabla^2 u) \end{aligned} \tag{5.2a}$$

$$\begin{aligned} &v_t + Uv_\xi + Vv_\eta \\ &= -(\xi_y p^*_\xi + \eta_y p^*_\eta) + \frac{1}{Re}(\nabla^2 v) \end{aligned} \tag{5.2b}$$

$$\xi_x u_\xi + \eta_x u_\eta + \xi_y v_\xi + \eta_y v_\eta = 0 \tag{5.3}$$

where (U, V) are the unscaled contravariant velocity components and defined as

$$U = \xi_x u + \xi_y v \tag{5.4a}$$

$$V = \eta_x u + \eta_y v \tag{5.4b}$$

and p^* is modified pressure defined by equation (4.7)

∇^2 is the transformed Laplacian operator and defined as

$$\begin{aligned}\nabla^2 q &= (\xi_x^2+\xi_y^2)q_{\xi\xi}+(\eta_x^2+\eta_y^2)q_{\eta\eta}\\ &+2(\xi_x\eta_x+\xi_y\eta_y)q_{\xi\eta}\\ &+(\xi_{xx}+\xi_{yy})q_\xi+(\eta_{xx}+\eta_{yy})q_\eta\end{aligned} \tag{5.5}$$

where q is arbitrary scalar quantity. ξ_x, ξ_y and so on appeared in equations (5.2)–(5.5) are the metrics of the grid. It should be noted that the transformed momentum equations (5.2) are not in the conservative form.

The basic algorithm is the same as that of the MAC method [9]. The discretization is made in the non-staggered grid, that is, all variables are defined in the intersections of grid lines. The present method is based on the time marching procedure and is divided into two stages.

On the first stage, velocity is updated by the momentum equations (5.2). The forward difference is used in time. The spatial differences are the fourth-order central difference for the convection terms and for the grid metrics terms and the second-order central difference for the pressure gradient terms. The fourth-derivative artificial numerical dissipation terms are added to the convection terms to stabilize computation. The resultant finite-difference equation for equation (5.2a) is

$$\begin{aligned}\frac{u_{i,j}^{n+1}-u_{i,j}}{\delta t} = &-U_{i,j}\frac{u_{i-2,j}-u_{i+2,j}-8(u_{i-1,j}-u_{i+1,j})}{12}\\ &-\beta(u_{i-2,j}+u_{i+2,j}-4(u_{i-1,j}+u_{i+1,j})+6u_{i,j})\\ &-V_{i,j}\frac{u_{i,j-2}-u_{i,j+2}-8(u_{i,j-1}-u_{i,j+1})}{12}\\ &-\beta(u_{i,j-2}+u_{i,j+2}-4(u_{i,j-1}+u_{i,j+1})+6u_{i,j})\\ &+\frac{1}{Re}[(\xi_{xi,j}^2+\xi_{yi,j}^2)(u_{i-1,j}-2u_{i,j}+u_{i+1,j})\\ &+(\eta_{xi,j}^2+\eta_{yi,j}^2)(u_{i,j-1}-2u_{i,j}-u_{i,j+1})\\ &+2(\xi_{xi,j}\eta_{xi,j}+\xi_{yi,j}\eta_{yi,j})\frac{u_{i+1,j+1}-u_{i+1,j-1}-u_{i-1,j+1}+u_{i-1,j-1}}{4}\\ &+(\xi_{xxi,j}+\xi_{yyi,j})\frac{u_{i+1,j}-u_{i-1,j}}{2}\end{aligned}$$

$$+(\eta_{xxi,j}+\eta_{yyi,j})\frac{u_{i,j+1}-u_{i,j-1}}{2}]$$

$$-\xi_{xi,j}\frac{p^*_{i+1,j}-p^*_{i-1,j}}{2} \tag{5.6}$$

$$-\eta_{xi,j}\frac{p^*_{i,j+1}-p^*_{i,j-1}}{2}$$

where superscript $n+1$ denotes the value at $(n+1)$-th step and superscripts n are dropped for simplicity. δt is the time increment and β is the parameter that determines the magnitude of the artificial dissipation.

On the second stage, pressure on the next time step is computed so that the velocity field on the next time step may satisfy the continuity condition. By taking divergence of the momentum equation s (5.2), the following Poisson equation for pressure is derived.

$$\begin{aligned}\nabla^2 p^* = \; & -\xi_x K_\xi - \eta_x K_\eta \\ & -\xi_y L_\xi - \eta_y L_\eta \\ & -D_t\end{aligned} \tag{5.7}$$

where

$$K = Uu_\xi + Vu_\eta - \frac{1}{Re}(\nabla^2 u)$$

$$L = Uv_\xi + Vv_\eta - \frac{1}{Re}(\nabla^2 v)$$

$$D = \xi_x u_\xi + \eta_x u_\eta + \xi_y v_\xi + \eta_y v_\eta$$

The right-hand-side of equation (5.7) is evaluated by the values at the present time step. The spatial differences for K and L are the same as those for equation (5.6). The time differential appeared in the last term is expressed by the forward difference. Then D, divergence of velocity, on the next time step is set zero from the continuity condition, while D on the present time step which is not necessarily zero due to numerical error is evaluated by the second-order central difference. This can eliminate the accumulation of numerical error [9]. The left-hand-side of equation (5.7) is evaluated by the second-order central difference and is solved iteratively by the Successive Over Relaxation method.

5.2 Free Surface Conditions

In this computation, the effects of viscosity and surface tension to the free surface conditions are neglected for simplicity. Therefore, the free surface conditions consist of the following two conditions. One is the pressure condition that means that pressure on the free surface is equal to atmospheric one or to prescribed value. The other is the kinematic condition that tells the fluid particles on the free surface keep staying on it. Because the grid points are not on the free surface in the present grid system, it is not easy to satisfy the free surface conditions on the exact location of the free surface.

The pressure condition is implemented in the solution process for the Poisson equation for pressure. To give the boundary condition at the intermediate point between grid points, where the free surface is located, the 'irregular stars method' used in the SUMMAC method [12] is extended to the curvilinear coordinates system.

The kinematic condition is used to determine the free surface shape in the time marching process. The wave elevation is defined in the computational coordinates as

$$\eta = h(\xi, t) \tag{5.8}$$

The kinematic condition is written as

$$h_t + U h_\xi - V = 0 \quad \text{on} \quad \eta = h \tag{5.9}$$

equation (5.9) is transformed into the finite-difference form in the same manner as that for the momentum equations (5.6). Velocity (U, V) on the free surface is extrapolated equally from the value at the adjacent lower grid points.

5.3 Other Boundary Conditions

The periodic boundary condition is used in the horizontal, $x-$, direction because the progressive periodic waves are considered. At the bottom of the computational domain, pressure and velocity are set equal to the values of the adjacent inner points.

6. Generation of Periodic Wave

To demonstrate the applicabilty of the method, the generation of the periodic progressive waves is numerically simulated. The proper initial and boundary conditions to generate periodic waves are discussed in this section.

The simplest initial condition is the still state, that is, velocity is zero and pressure is hydrostatic in the whole domain of computation. Alternative is to give an analytic solution of a periodic wave as the initial condition. In the latter case, the linear analytic solution for waves of infinitesimal amplitude is not adequate because

the linearized free surface condition of the theory is not consistent with the fully nonlinear free surface condition implemented in the numerical scheme. Analytic solutions for waves of finite amplitude such as Stokes theory can be used as the initial condition. The former condition, the still state, is used here for simplicity.

One way to generate waves is the oscillation of velocity and/or pressure in the inflow boundary[13]. This method simulates numerically a wave maker of a flap or piston type in an actual experimental tank. However, this approach cannot be adopted when the periodic condition is used in the horizontal direction, because the numerical wave maker generates waves which propagate in two, positive $x-$ and negative $x-$, directions. In case that the periodic condition is not used in space, the wave propagating in the direction oppsite to the computational domain does not affect the solution. However, with the periodic boundary condition, two waves propagating in the opposite directions affect each other and the solution differs from that for a single wave.

The other way is to give pressure distribution on a free surface. Periodic distribution of surface pressure that runs with the constant speed can generate the periodic progressive wave. This does not conflict with the periodic boundary condition of the scheme and is used here.

7. Numerical Results

7.1 Computational Conditions

Computational grid used is shown in Figure 9. The grid is orthogonal and consists of straight lines, though the present scheme can cope with the general curvilinear grid. The number of grid points is 51×51 and the computational domain is

$$0 \leq x \leq 1.02$$

$$-0.990668 \leq y \leq 0.2$$

The grid spacing in the horizontal direction is constant and 0.02, while that in the vertical direction is gradually varing from 0.01, the minimum value, to 0.10564, the maximum. The grid points are clustered near the free surface. The time increment δt is set 0.002 and the parameter β is set 0.1.

7.2 Results

The pressure distribution on the free surface is given by the following equation,

$$p^*(x, y, t) = gy + gw_a \cos(kx - \sigma t) \tag{5.10}$$

where (x, y) are the free surface location at time t and w_a is the amplitude of pressure oscilation defined with the dimension of water head. k is the wave number defined by the wave length λ as

$$k = \frac{2\pi}{\lambda}$$

and σ is the angular frequency of the wave. In the water waves, σ is related to the wave length by the following relationship,

$$\sigma = \sqrt{\frac{2\pi g}{\lambda}}$$

Here, the wave length λ of the generated wave is set 1.02 so that the computational domain in the horizontal direction is equal to one wave length and w_a is set 0.002. The velocity vector maps and the pressure distribution at various time steps are shown in Figure 10. The periodic wave is generated well. The pressure distribution beneath the free surface is smoothly connected to the pressure on the free surface. The velocity distributions show the approximately exponential decay in the depthwise direction. Figure 11 shows the time history of the wave elevation at $x = 0$. The wave amplitude becomes almost steady and nearly equal to 0.02 at $t = 8$. The computed wave amplitude is about ten times as large as w_a. Further investigation is required to explain the relation between w_a and the wave amplitude. The period of the computed wave is about 0.81 and is almost equal to that given in the surface pressure condition.

8. Conclusion

In part I, the fractional step method for incompressible fluid is presented together with some numerical results. The extension of the method to free surface problems are then made. The troubles encountered in the application of the method to free surface flow problem are discussed and finally some recommendations for computaion of the free surface flow using the fractional step method are made.

In part II, the numerical method based on the MAC method is applied to free surface problems. The boundary and initial conditions for the generation of periodic progressive waves are discussed. The computational results show that the wave that has the pre-determined wave length and frequency can be generated by the proper boundary and initial conditions.

The fractional step method has the advantage of the exact conservation of mass because it assures that the divergence-free condition is satisfied at each time

step. The MAC method is simpler than the fractional method. However, the mass conservation is satisfied only indirectly through the Poisson equation for pressure. Therefore, for applications that require the strict conservation of mass the fractional step method is preferable, though more efforts should be made to apply the fractional step method to free surface problems.

Acknowledgements

The first author was supported as a Fellow of the Science and Technology Agency of Japan during this work. The author also expresses his gratitude to the CFD group at the Ship Research Institute and Mr. Hung Le of Stanford University for their valuable input.

References

[1] Lee, C.H., Squires, K.D., Bertoglio, J.P., and Ferziger, J.H.,"Study of Lagrangian Characteristic Times using Direct Numerical Simulation", Symposium on Turbulent Shear Flows, Toulouse, France, August 1987.

[2] Moser, R.D., and Moin, P., "Direct Numerical Simulation of Curved Turbulent Channel Flow", Report TF-20, Department of Mechanical Engineering, Stanford University, Stanford, CA.

[3] Kim, J. and Moin P., "Application of Fractional-Step Method to Incompressible Navier-Stokes Equations", J. Comp. Phys., Vol. 59, pp. 308-323, 1984.

[4] Chorin, A.J., J. Comp. Phys., Vol. 2, 1967.

[5] Peyret, R., and Taylor, T.D., "Computational Methods for Fluid Flow", Springer-Verlag, 1983.

[6] Anderson, Tannehill, and Pletcher, "Computational Fluid Mechanics and Heat Transfer", McGraw-Hill, 1984.

[7] Lilly, D.K., Mon. Weather Rev., Vol. 93, 1965.

[8] Schreiber, R., Keller, H.B., J. Comp. Phys., Vol. 49, 1983.

[9] Harlow, F.H., and Welch, J.E., Phys. Fluids, Vol. 8, 1965.

[10] Hino, T., "Computation of a Free surface Flow around an Advancing Ship by the Navier-Stokes Equations", Pro. 5th Intern. Conf. Num. Ship Hydro., Hiroshima, Japan, September 1989.

[11] Hirt, C.W., and Shannon, J.P., "Free-Surface Stress Conditions for Incompressible-Flow Calculations", J. Comp. Phys., Vol. 2, pp. 403-411, 1968.

[12] Chan, R.K.-C., and Street, R.L., "A Computer Study of Finite-Amplitude Water Waves", J. Comp. Phys., Vol. 6, 1970.

[13] Hino, T., Miyata H. and Kajitani, H., "A Numerical Solution Method for Nonlinear Shallow Water Waves (First Report)", J. Soc. Nav. Arch. Japan, Vol.153,pp. 1-12, 1983.

Appendix A

For the staggered grid the pressure nodes are located one-half of a grid cell from the boundaries. Because of this the cosine series used to represent the pressure must be manipulated before fast transforms may be used. A cosine series for the variable ϕ with N points is

$$\phi_i = \sum_{l=0}^{N-1} \hat{\phi}_l \cos\frac{\pi l}{N}(i+\frac{1}{2})$$

$$i = 0, 1, \ldots, N-1 \qquad (A.1)$$

Multiplying (A.1) by $\cos(\pi l'(i+1/2)/N)$ and summing over i gives

$$\sum_{i=0}^{N-1} \phi_i \cos(\frac{\pi l'}{N}(i+\frac{1}{2})) =$$

$$\sum_{i=0}^{N-1}\sum_{l=0}^{N-1} \hat{\phi}_l \cos(\frac{\pi l}{N}(i+\frac{1}{2}))\cos(\frac{\pi l'}{N}(i+\frac{1}{2}))$$

$$= \sum_{l=0}^{N-1} \hat{\phi}_l \frac{1}{2} \sum_{i=0}^{N-1} [\cos\frac{\pi}{N}(l+l')(i+\frac{1}{2})$$

$$+\cos\frac{\pi}{N}(l-l')(i+\frac{1}{2})] \qquad (A.2)$$

To simplify this make use of the fact that the following quantity

$$\sum_{i=0}^{N-1} \cos\frac{\pi}{N}(i+\frac{1}{2})j$$

is equal to 0 if $j \neq 0$ and equal to N if $j = 0$. Therefore, for $l \neq l'$ A.2 is zero and for $l = l' \neq 0$:

$$\sum_{i=0}^{N-1} \cos\frac{\pi}{N}(l+l')(i+\frac{1}{2}) = 0$$

$$\sum_{i=0}^{N-1} \cos\frac{\pi}{N}(l-l')(i+\frac{1}{2}) = N$$

For $l = l' = 0$

$$\sum_{i=0}^{N-1} [\cos\frac{\pi}{N}(l+l')(i+\frac{1}{2}) + \cos\frac{\pi}{N}(l-l')(i+\frac{1}{2})] = 2N$$

thus

$$\hat{\phi}_l = \frac{2}{N} \sum_{i=0}^{N-1} \phi_i \cos\frac{\pi l}{N}(i+\frac{1}{2})$$

$$l = 0, 2, \ldots N-1 \qquad (A.3)$$

with a factor of 1/2 multiplying the coefficient for $\hat{\phi}_0$. Equation (A.3) can be rewritten as

$$\hat{\phi}_l = \frac{2}{N}\sum_{i=0}^{N-1}\phi_i[\cos\frac{\pi li}{N}\cos\frac{\pi l}{2N} - \sin\frac{\pi li}{N}\sin\frac{\pi l}{2N}] =$$

$$\frac{2}{N}(\sum_{i=0}^{N-1}\phi_i\cos\frac{\pi li}{N})\cos\frac{\pi l}{2N} - \frac{2}{N}(\sum\phi_i\sin\frac{\pi li}{N})\sin\frac{\pi l}{2N} \qquad (A.4)$$

Next consider the Fourier transform of the sequence of length $2N$

$$\phi_i = \sum_{l=-\frac{2N}{2}}^{\frac{2N}{2}-1}\tilde{\phi}_l e^{i\frac{2\pi}{2N}li}$$

$$i = 0, 1, \ldots, 2N-1$$

$$\tilde{\phi}_l = \frac{1}{2N}\sum_{i=0}^{2N-1}\phi_i e^{-i\frac{2\pi}{2N}li}$$

$$l = -\frac{2N}{2}, \ldots, 0, \ldots \frac{2N}{2} - 1 \qquad (A.5)$$

By choosing $\phi_i = 0$ for $i = N, N+1, \ldots, 2N-1$ $(A.5)$ becomes

$$\tilde{\phi}_l = \frac{1}{2N}\sum_{i=0}^{N-1}\phi_i e^{-i\frac{\pi li}{N}}$$

$$l = -N, \ldots, 0, \ldots, N-1$$

or

$$\tilde{\phi}_l = \frac{1}{2N}[(\sum_{i=0}^{N-1}\phi_i\cos\frac{\pi li}{N}) - i(\sum_{i=0}^{N-1}\phi_i\sin\frac{\pi li}{N})]$$

$$l = -N, \ldots, 0, \ldots, N-1 \qquad (A.6)$$

Comparing $A.6$ and $A.4$ gives

$$\hat{\phi}_l = \frac{2}{N}[\mathrm{Re}(\tilde{\phi}_l)\cos\frac{\pi l}{2N} + \mathrm{Im}(\tilde{\phi}_l)\sin\frac{\pi l}{2N}]$$

$$l = 0, 1, \ldots, N-1 \qquad (A.7)$$

Equation (A.7) gives the coefficients of the cosine series for the staggered grid. Similar manipulations are necessary for computing the function ϕ_i from the coefficients ϕ_l. The backward transform is given by:

$$\phi_i = \sum_{l=0}^{N-1}\hat{\phi}_l\cos\frac{\pi l}{N}(i + \frac{1}{2})$$

$$i = 0, 1, \ldots, N-1 \qquad (A.8)$$

Define the variable, ϕ_i^* as

$$\phi_i^* = \sum_{l=0}^{N-1} \hat{\phi}_l e^{i\frac{\pi l}{N}(i+\frac{1}{2})}$$

$$= \sum_{l=0}^{N-1} \hat{\phi}_l \cos\frac{\pi l}{N}(i+\frac{1}{2}) + i\sum_{l=0}^{N-1} \hat{\phi}_l \sin\frac{\pi l}{N}(i+\frac{1}{2})$$

$$i = 0, 1, \ldots, N-1 \qquad (A.9)$$

Thus $\phi_i = \mathrm{Re}(\phi_i^*)$

From $(A.9)$

$$\phi_i^* = \sum_{l=-N}^{N-1} \hat{\phi}_l e^{i\frac{2\pi}{2N}l(i+\frac{1}{2})}$$

$$= \sum_{l=-N}^{N-1} (\hat{\phi}_l \cos\frac{\pi l}{2N} + i\hat{\phi} + l\sin\frac{\pi l}{2N}) e^{i\frac{2\pi}{2N}li}$$

$$i = 0, 1, \ldots, N-1$$

if

$$\hat{\phi}_l = 0$$

for

$$l = -N, \ldots, -1$$

Thus, to summarize:

[1] Given a set of $\hat{\phi}_l$ (real), $l = 0, 1, \ldots N-1$

[2] Extend the sequence $\hat{\phi}_l$ to $2N$, $\hat{\phi}_l = 0$ for $l < 0$

[3] Calculate $\tilde{\phi}_l = \hat{\phi}_l \cos\frac{\pi l}{2N} + i\hat{\phi}_l \sin\frac{pil}{2N}$

[4] Backward transform $\tilde{\phi}_l, l = -N, \ldots, 0, \ldots, N-1$ to obtain ϕ_i^*

[5] ϕ_i will be the real part of ϕ_i^*.

Table 1 : Maximun error in the u velocity component after 30 steps.

Grid	Error
21×21	6.9724×10^{-5}
41×41	1.7588×10^{-5}

Table 2 : Stream function and vorticity at center of primary vortex for different Reynolds numbers.

Re	Present $\psi, (\omega)$ grid points	Kim and Moin [3] $\psi, (\omega)$ grid points	Schreiber and Keller [8] $\psi, (\omega)$ grid points
1	$-0.100, (-3.217)$ 65×65	$-0.099, (-3.316)$ 65×65	$-0.100, (-3.232)$ 121×121
400	$-0.112, (-2.257)$ 65×65	$-0.112, (-2.260)$ 65×65	$-0.113, (-2.281)$ 141×141
1000	$-0.116, (-2.030)$ 97×97	$-0.116, (-2.026)$ 97×97	$-0.116, (-2.026)$ 141×141
4000	$-0.112, (-1.804)$ 97×97	$-0.114, (-1.879)$ 97×97	$-0.112, (-1.805)$ 161×161

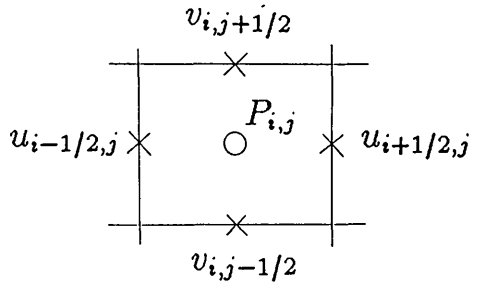

Fig. 1 Staggered grid in two dimensions.

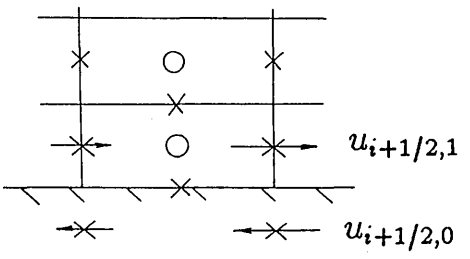

Fig. 2 Staggered grid near boundaries.

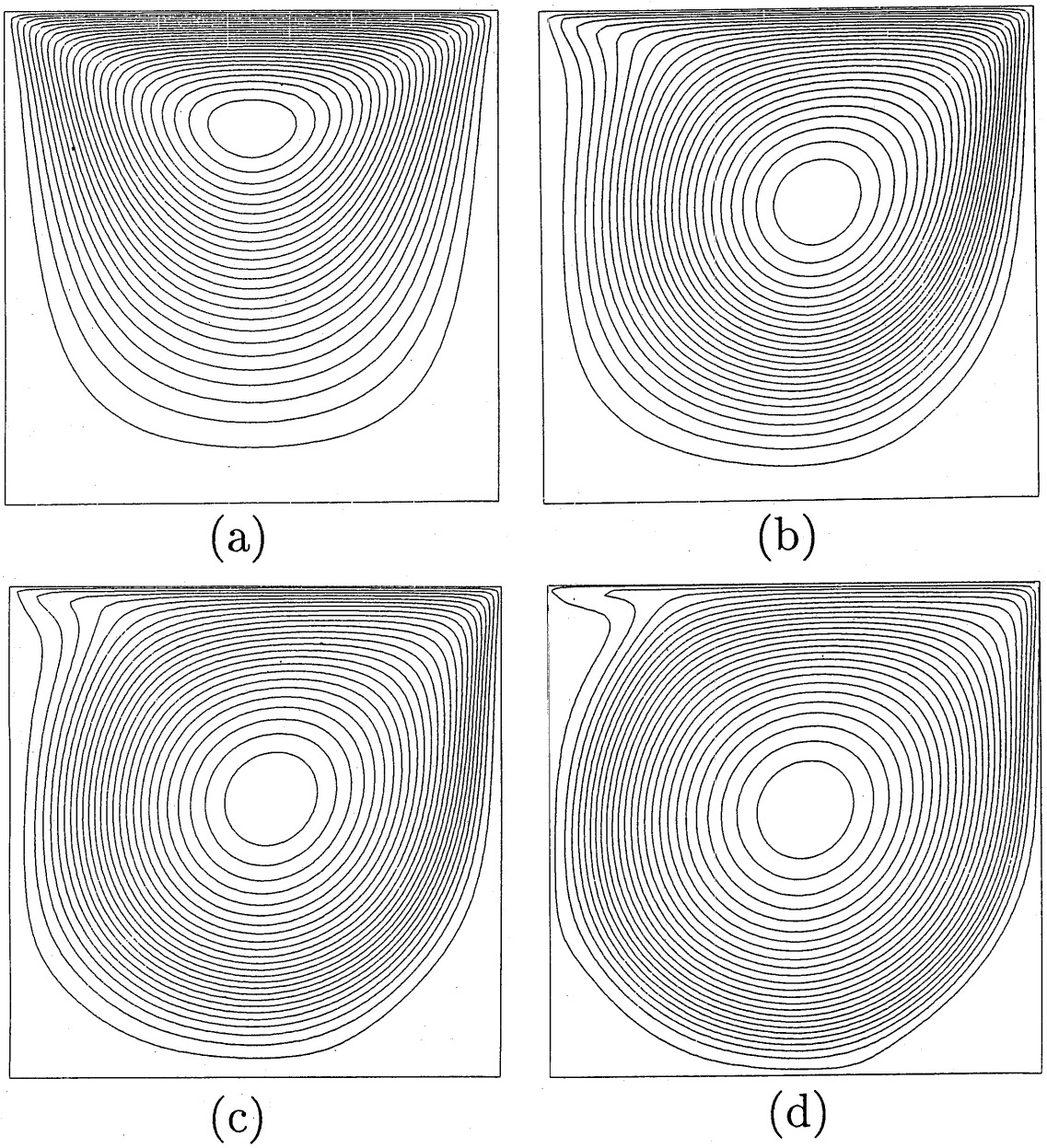

Fig. 3 Streamlines from cavity flow. (a) $Re=1$, (b) $Re=400$, (c) $Re=1000$, (d) $Re=4000$.

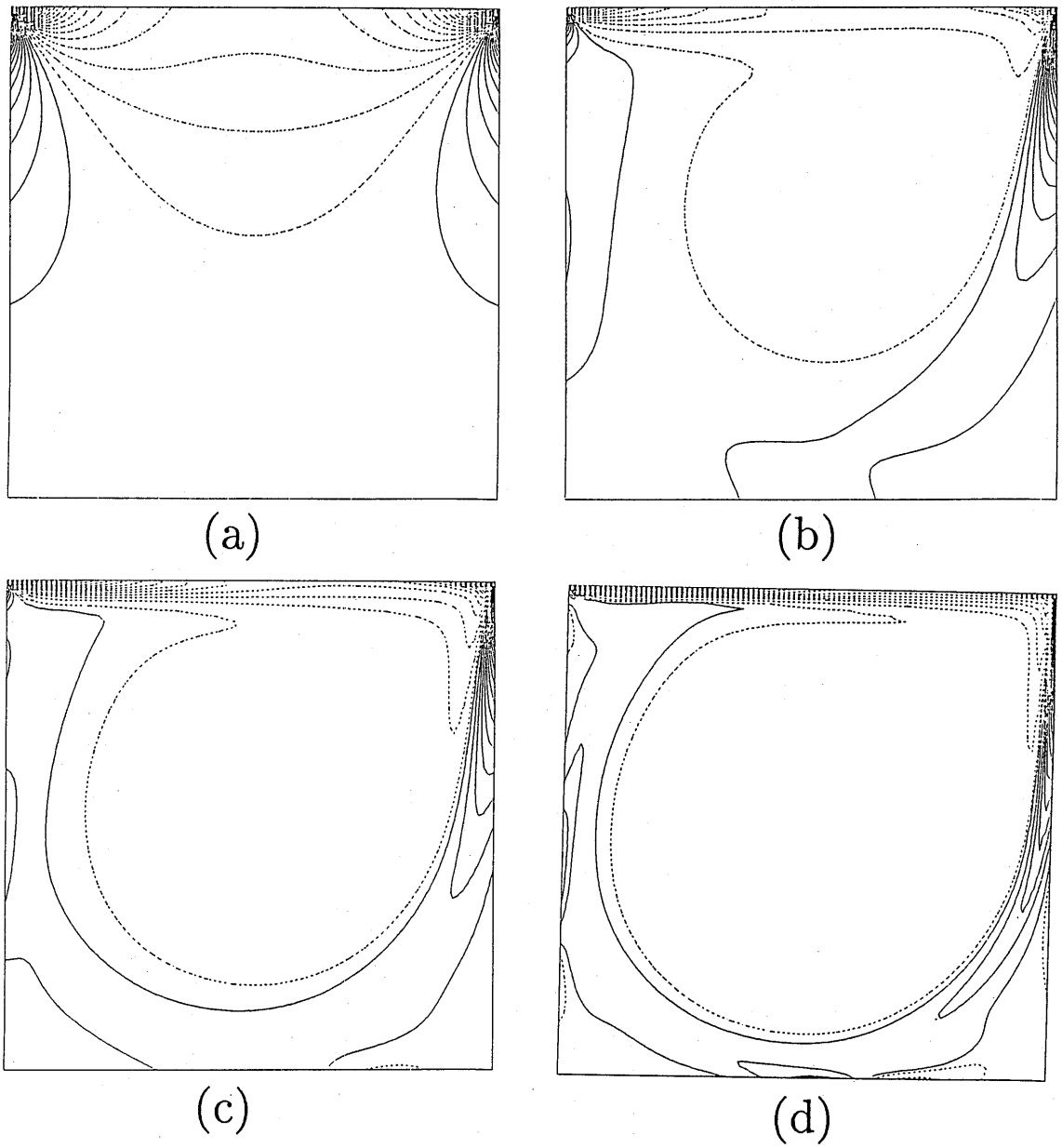

Fig. 4 Contours of constant vorticity from cavity flow. (a) $Re=1$, (b) $Re=400$, (c) $Re=1000$, (d) $Re=4000$.

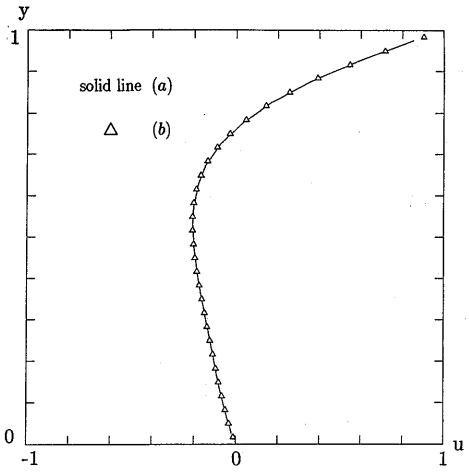

Fig. 5 Streamwise velocity profile at cavity midplane for $Re=1$. (a) 21×21, (b) 31×31.

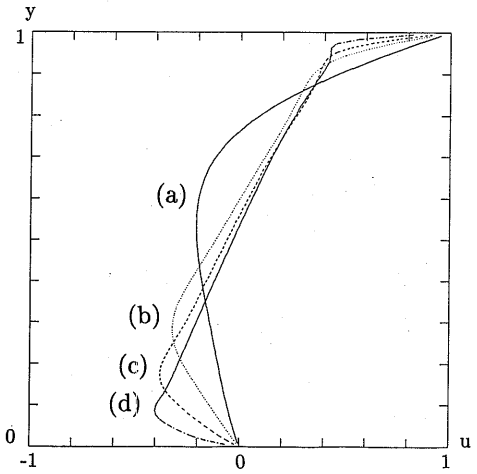

Fig. 7 Streamwise velocity profiles at cavity midplane for (a) $Re=1$, (b) $Re=400$, (c) $Re=1000$, (d) $Re=4000$.

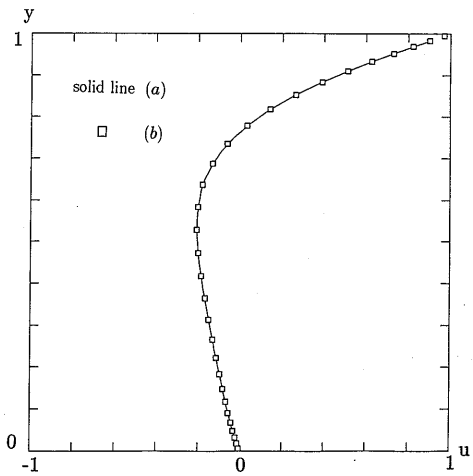

Fig. 6 Streamwise velocity profile at cavity midplane for $Re=1$, 31×31. (a) uniform grid, (b) non-uniform grid.

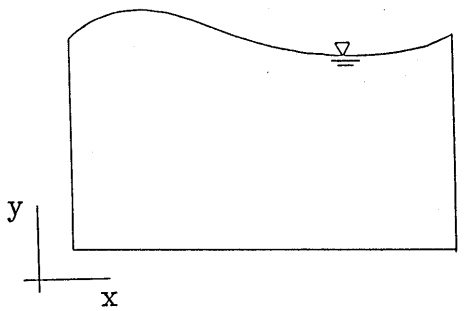

Fig. 8 Geometry of free surface flow.

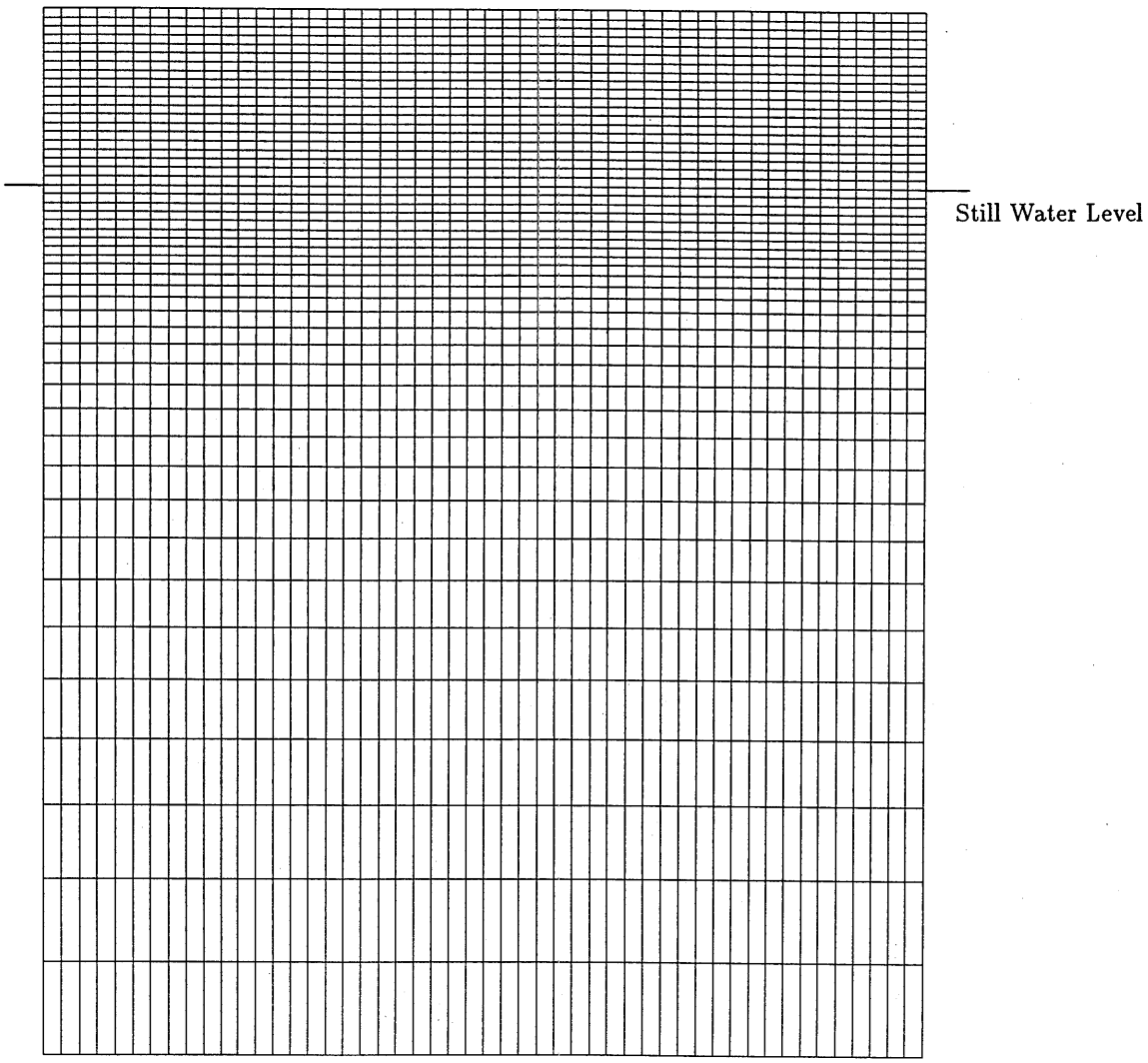

Fig. 9 Compuataional grid for periodic wave generation.

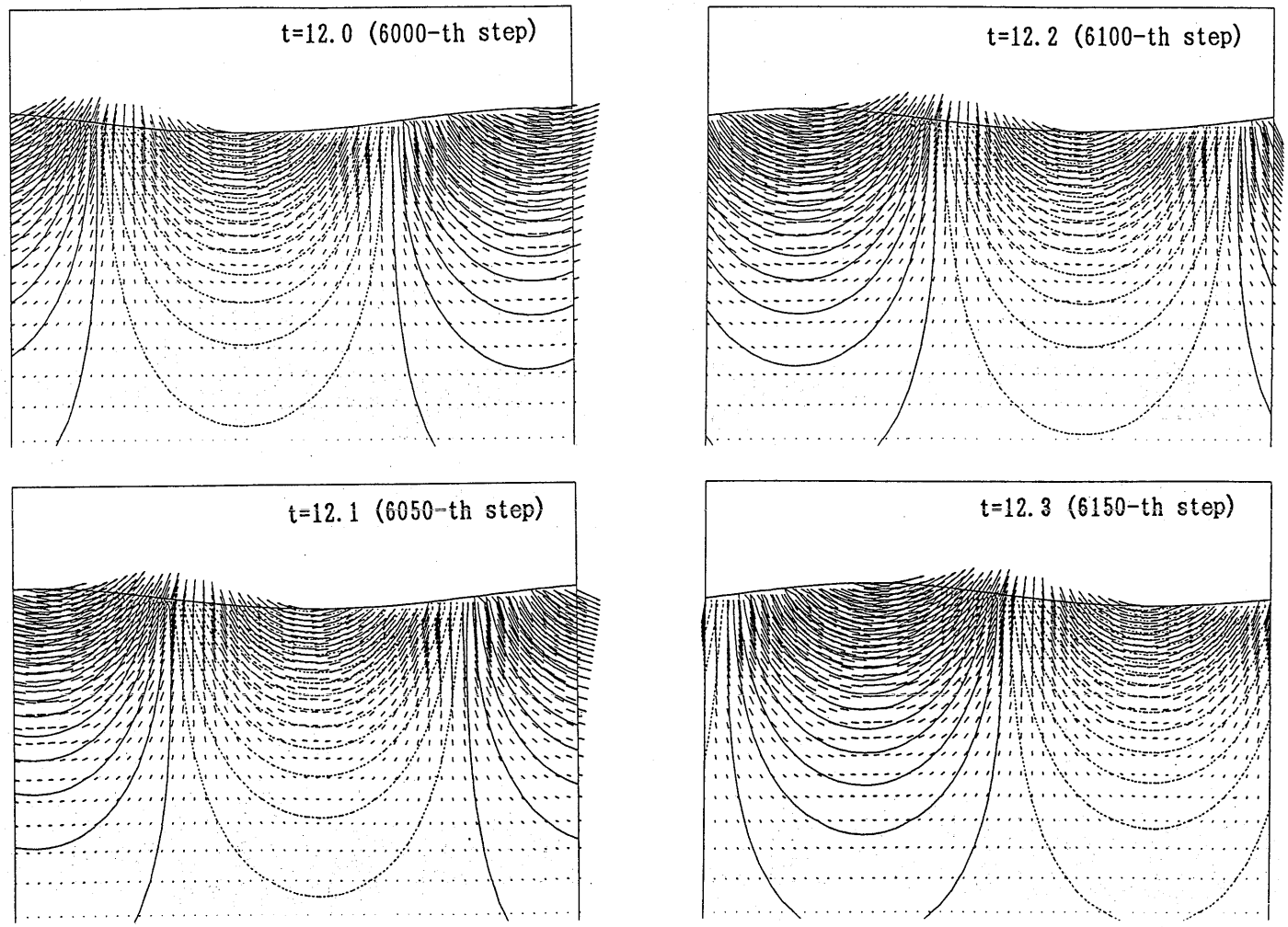

Fig. 10a Velocity vectors and pressure contours on various time steps.

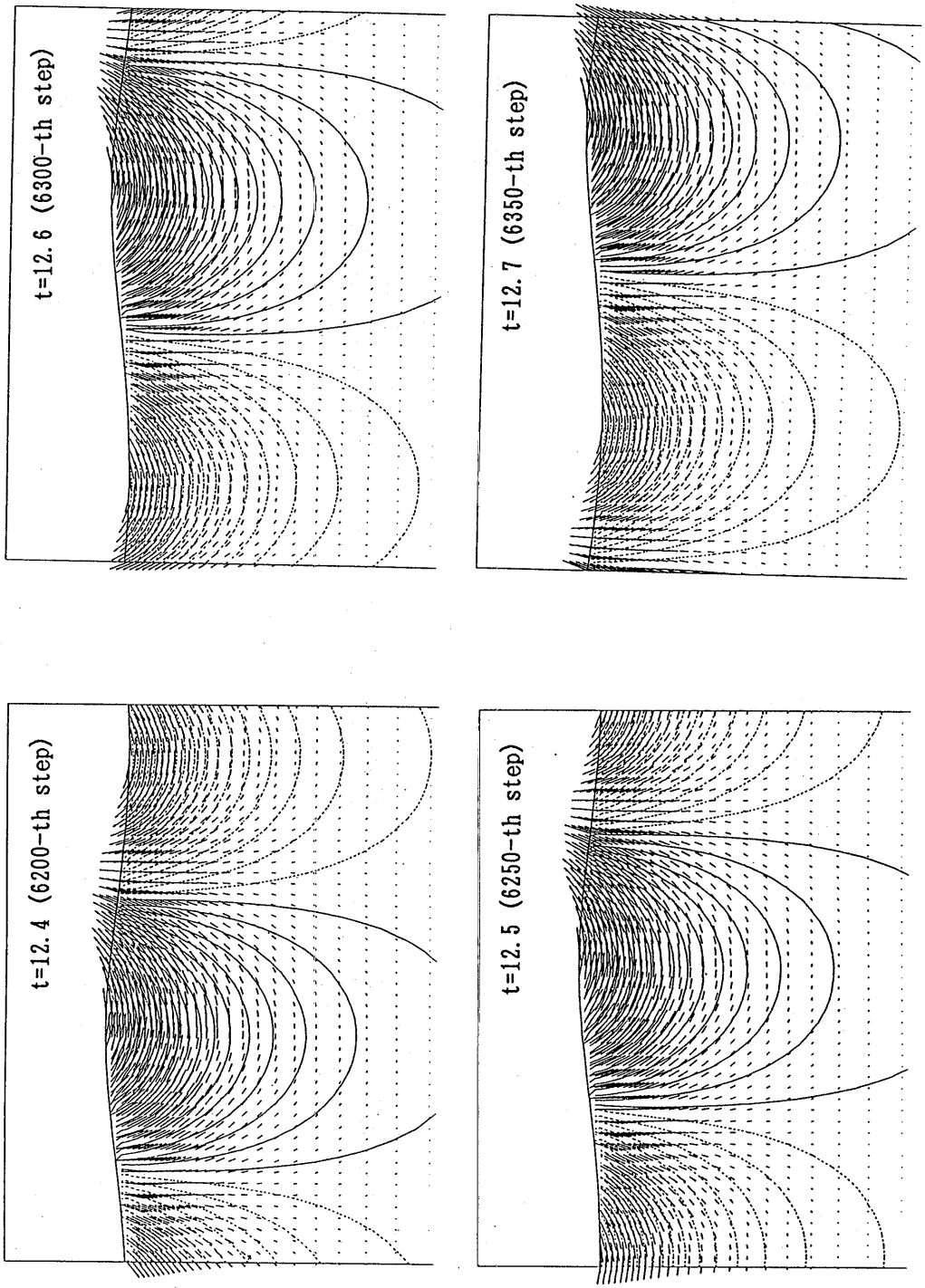

Fig. 10b (continued from Fig.10 a).

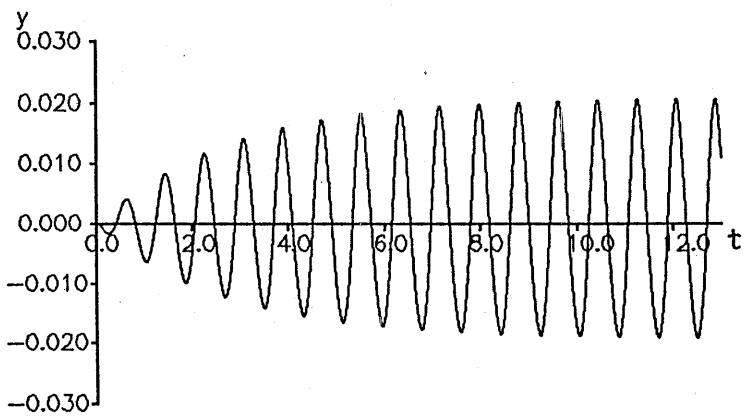

Fig. 11 Time history of wave elevation at $x=0$.